



Enhancing Electrochemical Performance through Swift Functional Group Tuning of MXenes

Penghui Cui,^[a] Hejing Wang,^[b] Bowen Yang,^[c] Shu Dong,^[a] Menggai Jiao,^[b] Ruizheng Zhao,^[b] Kai Zhu,^[a] Yong-Zheng Fang,*^[b] Zhen Zhou,^[b] and Dianxue Cao*^[a]

Chemical manipulation of surface functional groups on two-dimensional transition metal carbides and/or nitrides (MXenes) provides a wide range of design and application prospects. However, achieving rapid targeted modification of surface groups remains a significant challenge. Herein, we propose a general strategy to swiftly shear and customize surface groups on $Ti_3C_2T_x$ -MXene via the flash Joule heating (FJH) reaction within 1 s. Successfully, MXenes with 9 target terminations, including VII A (F, Cl, Br, or I), VI A (O, S, or Se), and V A (N or P),

either single or multiple, are synthesized, with a surface content of up to about 76%. The impact of these terminations is systematically analyzed on electrochemical performance, demonstrating that VI A and V A terminations have higher electrochemical activity than VII A. Particularly, N-, S-, and O-terminated MXenes exhibit enhanced specific capacities and undecayed cycling performance. These findings offer valuable insights for the surface engineering design and performance optimization of functional materials.

Introduction

Surface chemical modification of nanomaterials has a significant influence on their physical and chemical properties, rendering it widely used in the functional customization of materials.^[1–4] Two-dimensional (2D) transition metal carbides and/or nitrides (MXenes), in contrast to other 2D materials with non-active surfaces such as graphene and boron nitride, have attracted wide attention due to their abundant surface groups.^[5–7] These groups are typically derived from the MXenes preparation process, wherein the A atomic layer in the MAX phase precursor (M represents a transition metal element, A indicates a main group element from 13–16 Å, and X is carbon and/or nitrogen) is selectively etched to synthesize MX. Meanwhile, the exposed MX surface is terminated by anions present in the etching solution (commonly –F, –OH, –O, and –Cl), denoted as T_x .^[8] In

electrochemical processes, these surface groups can function as redox centers or mediums to provide a large amount of surface pseudocapacitive capacity,^[9–13] which makes MXenes promising anode materials for high-rate lithium-ion batteries (LIBs) and lithium-ion capacitors (LICs).

The surface chemistry and electrochemical performance of MXenes can be controlled by adjusting the species and concentrations of surface groups, such as electrolyte wettability,^[14] double electric layer structure,^[15] and cationic diffusivity and storage capacity.^[11,16] Zhao et al. simulated the diffusion-adsorption of halogen anions on the $Ti_3C_2T_x$ surfaces using molecular dynamics and found that excellent ionic diffusion performance is conducive to designing superior electrode materials.^[17] Jing et al. achieved N-termination modification by attaching 4-nitrobenzene groups to the $Ti_3C_2T_x$ surface via a nitrogen fixation reaction, resulting in a tunable work function window for $Ti_3C_2T_x$.^[18] Gupta et al. used microwave heating to achieve P doping in $Ti_3C_2T_x$, effectively increasing the surface redox sites and the layer spacing for higher pseudocapacitive storage.^[19]

However, the exchange reaction of surface terminations typically requires high temperatures of hundreds or even thousands of Kelvin and long reaction times using conventional solvent methods.^[20–22] Although Lewis acidic molten salt has been proposed and successfully utilized for tailoring halogen terminations,^[1] efficiently linking chalcogen and pnictogen terminations to MXenes surface remains difficult due to the high melting points of their compounds. In addition, MXenes are highly susceptible to oxidation at a prolonged high-temperature reaction over several hours.^[23] Therefore, it remains a great challenge to achieve fast and efficient tuning of surface functional groups as well as elucidate the electrochemical effects associated with surface groups.

Herein, we proposed a general strategy for rapidly modifying the surface groups on the $Ti_3C_2T_x$ via flash Joule heating (FJH) reaction within 1 s.^[24–26] The application of high-energy

[a] P. Cui, S. Dong, Prof. K. Zhu, Prof. D. Cao
Key Laboratory of Superlight Materials and Surface Technology (Ministry of Education)

College of Material Science and Chemical Engineering, Harbin Engineering University
Harbin 150001, China
E-mail: caodianxue@hrbeu.edu.cn

[b] H. Wang, Dr. M. Jiao, Dr. R. Zhao, Dr. Y.-Z. Fang, Prof. Z. Zhou
Department: Interdisciplinary Research Center for Sustainable Energy Science and Engineering (IRC4SE²)
Zhengzhou University, School of Chemical Engineering, Zhengzhou University, Zhengzhou 450001, Henan, China
E-mail: fangzhengnano@163.com

[c] Dr. B. Yang
Key Laboratory of Cold Region Urban and Rural Human Settlement Environment Science and Technology, Ministry of Industry and Information Technology
School of Architecture and Design, Harbin Institute of Technology
Harbin 150001, China

 Supporting information for this article is available on the WWW under
<https://doi.org/10.1002/batt.202400274>

electrical pulses directly traverses MXenes, generating instantaneous high temperatures of up to 500~3000 K,^[27] thereby enabling controlled shear and modification of the primitive surface terminations on MXenes. Significantly, 9 target terminations, including VII A (F, Cl, Br, or I), VI A (O, S, or Se), and V A (N or P), either unitary, binary, or ternary, are successfully linked with MXenes with a surface content of up to about 76%. Furthermore, the important role of these surface terminations in electrochemistry is investigated systematically, demonstrating that VI A and V A terminations generally exhibit superior performance to VII A.

Results and Discussion

The schematic process of the $\text{Ti}_3\text{C}_2\text{T}_x$ -MXene terminations exchange via the FJH reaction is shown in Figure 1a. First, $\text{Ti}_3\text{C}_2\text{T}_x$ was prepared through the typical HCl/LiF etching method, which facilitates the production of 2D MXenes with a few- or single-layer structure.^[28-29] The obtained $\text{Ti}_3\text{C}_2\text{T}_x$ nanosheets were observed by transmission electron microscopy (TEM, Figure S1), presenting an ultrathin structure with fewer than 5 layers and abundant $-\text{F}$, $-\text{Cl}$, and $-\text{O}$ -containing surface groups. After that, the $\text{Ti}_3\text{C}_2\text{T}_x$ sample was positioned between two graphite electrodes enclosed in a quartz tube. A low vacuum environment (-0.1 MPa) was applied to the system to inhibit $\text{Ti}_3\text{C}_2\text{T}_x$ oxidation and facilitate outgassing. A parallel capacitor bank (Figure S2) was connected to the graphite electrodes to provide a high-voltage current through the sample (Figure 1b), inducing an instantaneous high temper-

ature of several thousand K within 1 s due to the Joule-heating effect.^[30] The ultrahigh temperature enables the shearing of weak primitive groups on Ti_3C_2 , leading to a substantial gas release and resulting in a microscopic explosion with a flash (Figure 1c). The obtained product is named flash $\text{Ti}_3\text{C}_2\text{T}_x$ ($\text{F-Ti}_3\text{C}_2\text{T}_x$). When mixing various modifying agents with low decomposition temperatures, a chemical environment containing a large number of target elements can be established at high temperatures. Consequently, the surface functional group on $\text{Ti}_3\text{C}_2\text{T}_x$ will be rapidly modified due to the exchange reaction between the primitive thermally unstable groups and target elements under high temperatures (Figure 1a).

To investigate the change of primitive groups (major $-\text{O}$, $-\text{F}$, and $-\text{OH}$) on the Ti_3C_2 surface during the FJH process, their bonding strength was first analyzed by first-principles computations. As shown in Figures 2a and S3, Ti_3C_2 exhibits the most negative adsorption energy for $-\text{O}$ (-9.758 eV), followed by $-\text{F}$ and $-\text{OH}$ groups (-7.069 and -6.062 eV, respectively), implying that $-\text{O}$ termination is more thermodynamically stable, while $-\text{OH}$ groups will be sheared first, which has been identified as detrimental to Li-ion storage.^[16] By adjusting the discharge voltage and the number of capacitors, the electric energy and reaction temperature of the FJH can be accurately controlled (discharge parameters are listed in Table S1). With increasing the energy from 60 to 500 J, the signals of $-\text{OH}/\text{H}_2\text{O}$ around 3450 cm^{-1} and $\text{C}-\text{F}$ at 1050 cm^{-1} in Fourier transform infrared (FTIR) spectra gradually decrease (Figure 2b).^[31-32] This confirms that $-\text{OH}$ and $-\text{F}$ can be sheared by the FJH technique, supporting the results of first-principles computations.

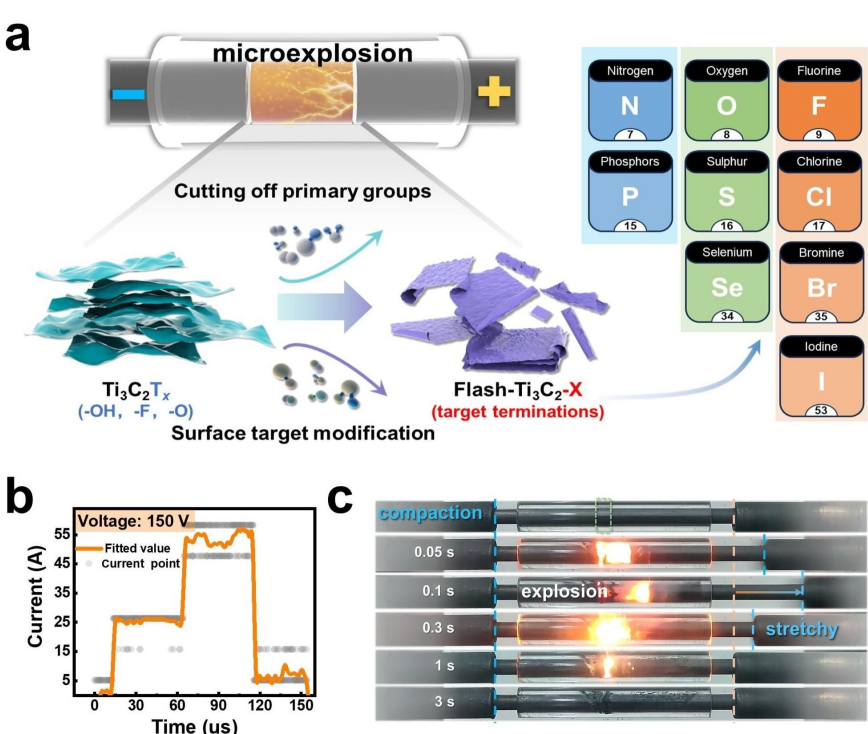


Figure 1. Surface functional groups tuning of $\text{Ti}_3\text{C}_2\text{T}_x$ -MXene by FJH reactions. (a) Schematic process and 9 target terminations; (b) Current flowing across the $\text{Ti}_3\text{C}_2\text{T}_x$ sample under 150 V voltage and 120 J electric energy; (c) Digital images during the FJH reaction, with micro-explosion and flash phenomena.

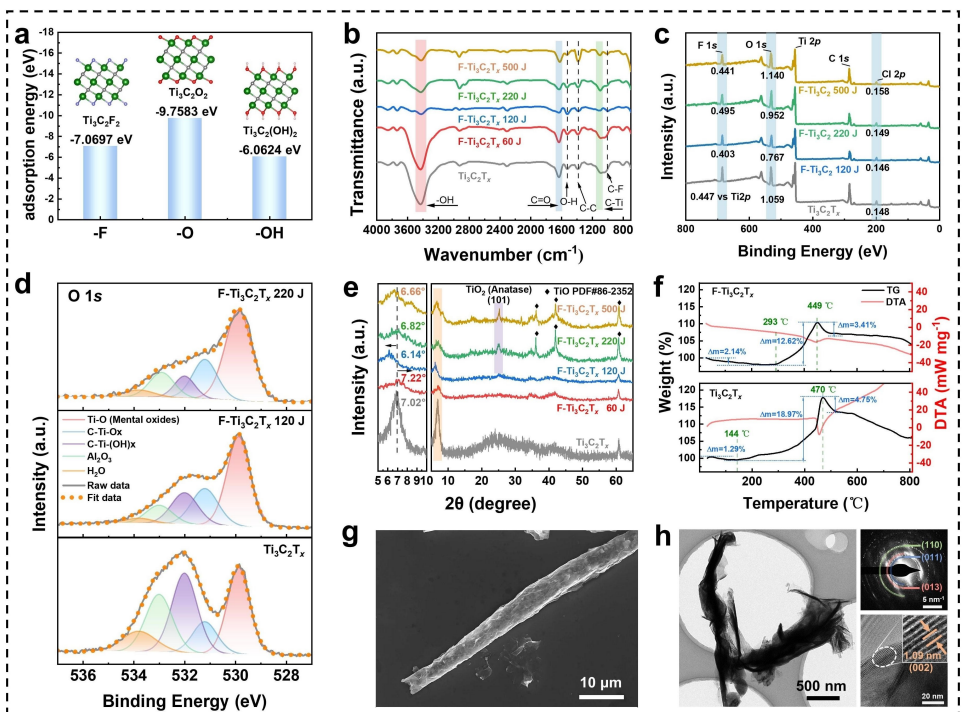


Figure 2. Surface chemistry, structure, and morphology changes of F–Ti₃C₂T_x during the FJH reaction. (a) Adsorption energy calculation of Ti₃C₂ for –F, –O, and –OH groups; (b) FTIR, (c) XPS, (d) O 1s XPS, and (e) XRD patterns of original Ti₃C₂T_x and F–Ti₃C₂T_x synthesized under different electric energies; (f) Thermogravimetric analysis of original Ti₃C₂T_x and F–Ti₃C₂T_x (120 J) at atmosphere; (g) SEM and (h) TEM images of F–Ti₃C₂T_x (120 J), with diffraction patterns of Ti₃C₂ (110), (013), and (011) crystal face, and an increased (002) lattice fringe.

The surface groups were further quantitatively analyzed by X-ray photoelectron spectroscopy (XPS), showing F 1s, O 1s, Ti 2p, C 1s, and Cl 2p signal peaks around 685, 532, 456, 285, and 199 eV, respectively (Figure 2c).^[33–34] Compared with the original Ti₃C₂T_x, the F–Ti₃C₂T_x obtained under 120 J exhibits a decrease in the content of O and F (relative to Ti). Abnormally, when the energy reaches 500 J, there is a relative increase in the surface content of O and F, implying that F–Ti₃C₂T_x undergoes oxidation and both F and O participate in the surface reaction. This suggests that solely increasing the electric energy is not effective in eliminating surface groups. The high-resolution spectra of O 1s and C 1s (Figures 2d and S4) reveal that the –OH and carboxyl terminations are clearly clipped through the FJH reaction, along with an enhanced Ti–C bond (peak locations are detailed in Table S2).^[35–36] However, when energy increase to 220 J, the Ti–O bond belonging to titanium oxide is found to be significantly enlarged in the O 1s and Ti 2p spectra (Figure S5), and the Ti–O–F bond is also detected in the F 1s spectrum (Figure S6).^[37] This suggests that –F and long-chain O-containing groups can be sheared at 120 J, but they will also oxidize surface Ti atoms under excessive electric energies.

The crystal changes of the Ti₃C₂T_x before and after the FJH reaction are analyzed by X-ray diffraction (XRD) patterns (Figure 2e). The original Ti₃C₂T_x (black) exhibits a typical (002) peak at 7.02° without the characteristic peak of Ti₃AlC₂–MAX precursor, confirming the successful preparation of Ti₃C₂T_x–MXene.^[38–40] After the FJH reaction, the (002) peak of the F–Ti₃C₂T_x obtained under 120 J (blue) significantly shifts to the left (6.14°), which is attributed to the interlayer explosion

caused by the gasification of unstable groups (Figure 1c). For comparison, the (002) peak of F–Ti₃C₂T_x (60 J, red) is slightly shifted to the right, corresponding to a decrease in interlayer spacing. This suggests that the surface groups were not effectively removed under 60 J, which is consistent with the results of the FTIR spectra. While the reduced layer spacing could be attributed to the removal of interlayer water. When reaction energy is excessive (220 J, green; 500 J, yellow), Ti₃C₂T_x will be oxidized and the characteristic peaks of titanium oxide are detected at 25.1° (anatase TiO₂) and 36.2°, 42.1°, and 60.9° (TiO). The source of the oxygen could be attributed to the decomposition of surface oxygen-containing groups and the interlayer water molecules. Due to the limited oxygen and hydrogen, the formation of TiO in low oxidation state is more dynamically favorable compared to TiO₂ in high oxidation state. Additionally, numerous large spheres could be observed on the Ti₃C₂T_x (500 J, Figure S7), accompanied by F and O aggregation. This demonstrates that the presence of –F will also stimulate the oxidation of MXenes at excessively high temperatures. Therefore, the FJH process should be carried out under the conditions below 220 J electric energy to ensure that the Ti₃C₂T_x does not undergo a phase transition.

The thermal stability of the F–Ti₃C₂T_x (120 J) was studied by thermogravimetric tests in air. As shown in Figure 2f, the F–Ti₃C₂T_x exhibits a higher mass increase temperature (293 °C), marking the beginning of MXenes oxidation, and a smaller mass change between 200 to 500 °C, compared with the original Ti₃C₂T_x (144 °C). This demonstrates that the removal of –OH and –F terminations improves the thermal stability of

MXenes. Reiterated experiments consistently demonstrated that $\text{Ti}_3\text{C}_2\text{T}_x$ exhibited less mass loss compared to $\text{F}-\text{Ti}_3\text{C}_2\text{T}_x$ before 200°C. This result may be attributed to the premature oxidation of $\text{Ti}_3\text{C}_2\text{T}_x$, resulting in a mass increase before 200°C and thus leading to a lower content detection of the adsorbed water compared to $\text{F}-\text{Ti}_3\text{C}_2\text{T}_x$. Scanning electron microscopy (SEM, Figure 2g) and TEM (Figure 2h) show the morphology of $\text{F}-\text{Ti}_3\text{C}_2\text{T}_x$. Interestingly, after the FJH reaction, $\text{F}-\text{Ti}_3\text{C}_2\text{T}_x$ displays a three-dimensional (3D) rod or tube structure with increased interlayer space. This curling behavior during the FJH process may be caused by the increased surface energy of MXenes resulting from the removal of lots of surface functional groups.^[41] These findings suggest that the FJH technology has the ability to regulate material surface chemistry, structure, and morphology.

When mixing $\text{Ti}_3\text{C}_2\text{T}_x$ with modifying agents during the FJH reaction, the target modification of functional terminations can be achieved within 1 s; the synthesized product is named $\text{F}-\text{Ti}_3\text{C}_2-\text{X}$ (X represents target terminations). The modifying agents and reaction conditions are shown in Table S3. At high temperatures, the target elements will vaporize and replace the unstable –F and –OH terminations (Figure 3a). Figure 3b–j shows the SEM images of the $\text{F}-\text{Ti}_3\text{C}_2-\text{X}$, including VII A ($\text{Ti}_3\text{C}_2-\text{F}$, Cl, Br, or I), VI A ($\text{Ti}_3\text{C}_2-\text{O}$, S, or Se), and V A ($\text{Ti}_3\text{C}_2-\text{N}$ or P). The unaltered sheet morphology indicates that the surface energy of $\text{F}-\text{Ti}_3\text{C}_2-\text{X}$ does not evidently increase, implying that the Ti_3C_2 surface is terminated by target elements. Energy-dispersive

spectroscopy (EDS) mapping (insert in Figure 3) demonstrates a uniform distribution of target elements, confirming the effectiveness of regulating MXene surface group via the FJH reaction. Notably, in addition to regulating a kind target termination, the simultaneous design of multiple terminations can also be achieved by selecting modifying agents containing multiple target elements, as demonstrated by the synthesized $\text{Ti}_3\text{C}_2-\text{N}$, S (Figure S8) and $\text{Ti}_3\text{C}_2-\text{N}$, Br (Figure 3k). This opens vast possibilities for tuning physicochemical properties and electrochemical performance of MXenes through manipulating multiple surface functional groups. The proportion of these target terminations on the Ti_3C_2 surface was analyzed through normalization treatment of surface content (Figure 3n and Table S4). Among these, $\text{F}-\text{Ti}_3\text{C}_2-\text{O}$ presents the highest surface content for target –O, reaching an impressive 76% coverage. Moreover, the target F-termination can account for as much as 48% on $\text{F}-\text{Ti}_3\text{C}_2-\text{F}$ and the additional terminations can be introduced up to 23% on the $\text{F}-\text{Ti}_3\text{C}_2-\text{N}$ surface. Note that the –O termination is the most stable on Ti_3C_2 , and the washing process further increases the content of the oxygen-containing group on Ti_3C_2 , resulting in a larger proportion of –O terminations in all $\text{F}-\text{Ti}_3\text{C}_2-\text{X}$. In addition, the surface percentage of termination is also directly related to atomic size and volatility, with larger atomic radius and easily volatile elements exhibiting lower surface content, such as Br, I and S. The content of the target element in the modifying agent is also

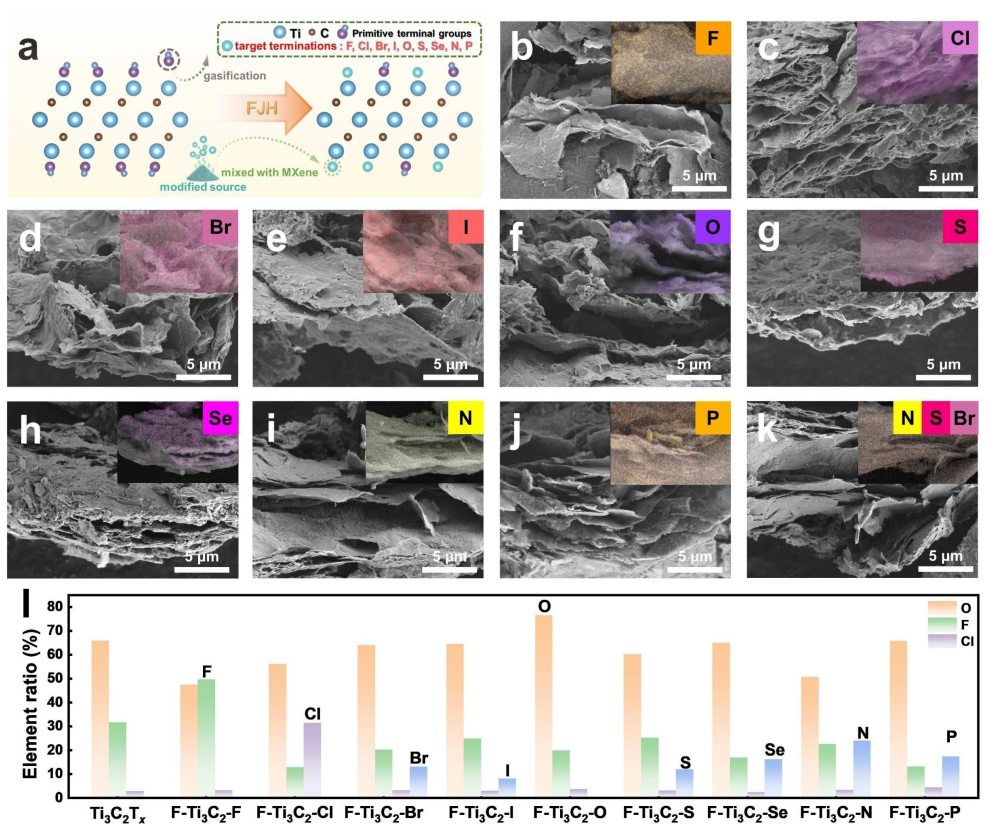


Figure 3. Target modification of functional terminations on $\text{Ti}_3\text{C}_2\text{T}_x$ surface. (a) Schematic of surface termination exchange; (b–k) SEM images of $\text{F}-\text{Ti}_3\text{C}_2-\text{X}$, including VII A ($\text{Ti}_3\text{C}_2-\text{F}$, Cl, Br, or I), VI A ($\text{Ti}_3\text{C}_2-\text{O}$, S, or Se), and V A ($\text{Ti}_3\text{C}_2-\text{N}$ or P); (l) Normalized surface elemental ratio of original $\text{Ti}_3\text{C}_2\text{T}_x$ and 9 $\text{F}-\text{Ti}_3\text{C}_2-\text{X}$.

critical because it affects the target termination concentration involved during the FJH reaction.

To investigate the influence of surface functional groups on electrochemical performances, the synthesized $\text{F-Ti}_3\text{C}_2\text{-X}$ was employed as an anode for Li-ion storage (see Methods for detail). Figure S9 shows the rate performance of $\text{Ti}_3\text{C}_2\text{T}_x$ before and after the FJH reaction, in which $\text{F-Ti}_3\text{C}_2\text{T}_x$ (120 J) displays improved specific capacities and rate performance compared to the original $\text{Ti}_3\text{C}_2\text{T}_x$, indicating that the reduction of $-\text{OH}$ and $-\text{F}$ terminations enhances the electrochemical performances of MXenes. After directionally adjusting functional terminations, the electrochemical effects of different terminations can be analyzed concretely. Figure 4a presents the average discharge specific capacities of the 9 $\text{F-Ti}_3\text{C}_2\text{-X}$ at 50, 500, and 2000 mA g^{-1} , based on their rate tests shown in Figure S10. It can be revealed that VII A and V A terminations generally exhibit higher capacities than VII A, and $\text{F-Ti}_3\text{C}_2\text{-Br}$, $\text{F-Ti}_3\text{C}_2\text{-S}$, and $\text{F-Ti}_3\text{C}_2\text{-N}$ demonstrate superior rate performance within their respective main groups. Among them, $\text{F-Ti}_3\text{C}_2\text{-N}$ exhibits the highest capacities of 288, 235, and 188 mAh g^{-1} at 50, 500, and 2000 mA g^{-1} , respectively, which are significantly higher than those of the original $\text{Ti}_3\text{C}_2\text{T}_x$, highlighting the important role of functional groups. The charge-discharge curves of the capable $\text{F-Ti}_3\text{C}_2\text{-N}$, $\text{F-Ti}_3\text{C}_2\text{-S}$, $\text{F-Ti}_3\text{C}_2\text{-O}$, and $\text{F-Ti}_3\text{C}_2\text{-Br}$ resemble that

of the original $\text{Ti}_3\text{C}_2\text{T}_x$ (Figure 4b), indicating a similar pseudocapacitive charge storage mechanism.

To gain insights into the electrochemical kinetics of different terminations, initial electrochemical impedance spectroscopy (EIS) of $\text{F-Ti}_3\text{C}_2\text{-X}$ was further analyzed (Figure 4c). At high frequencies, $\text{F-Ti}_3\text{C}_2\text{-Cl}$ exhibits the smallest arc followed by $-\text{O}$ and $-\text{N}$, suggesting quick charge transfer processes, while $\text{F-Ti}_3\text{C}_2\text{-S}$ presents an arc composed of several semicircles, suggesting $-\text{S}$ provides multiple charge transfer processes, which are conducive to high capacity. Additionally, the Warburg coefficient (σ), reflecting Li-ion diffusion rate in electrode materials,^[42] was calculated from the relation of $Z' \cdot \omega^{-1/2}$ for those $\text{F-Ti}_3\text{C}_2\text{-X}$ (Figure 4d), where a smaller σ -value indicates a larger diffusion rate. Among all terminations, $\text{F-Ti}_3\text{C}_2\text{-S}$ and $-\text{Br}$ exhibit the largest Li-ion diffusion rates, while $-\text{N}$ and $-\text{F}$ show the smallest rates. This is closely associated with the electronegativity of terminations and their binding energy with Li, where too large binding energy will restrict Li-ion diffusion capacity, while too small binding energy will lead to a small Li adsorption capacity. The charge storage mechanism of the 9 $\text{F-Ti}_3\text{C}_2\text{-X}$ is further analyzed by the cyclic voltammetry (CV, Figure S11) test, where different terminations exhibit distinct CV curves. Especially, the S and Se elements show multiple oxidation-reduction peaks, implying conversion mechanisms favour high capacity. However, the reversibility of $\text{F-Ti}_3\text{C}_2\text{-Se}$ is

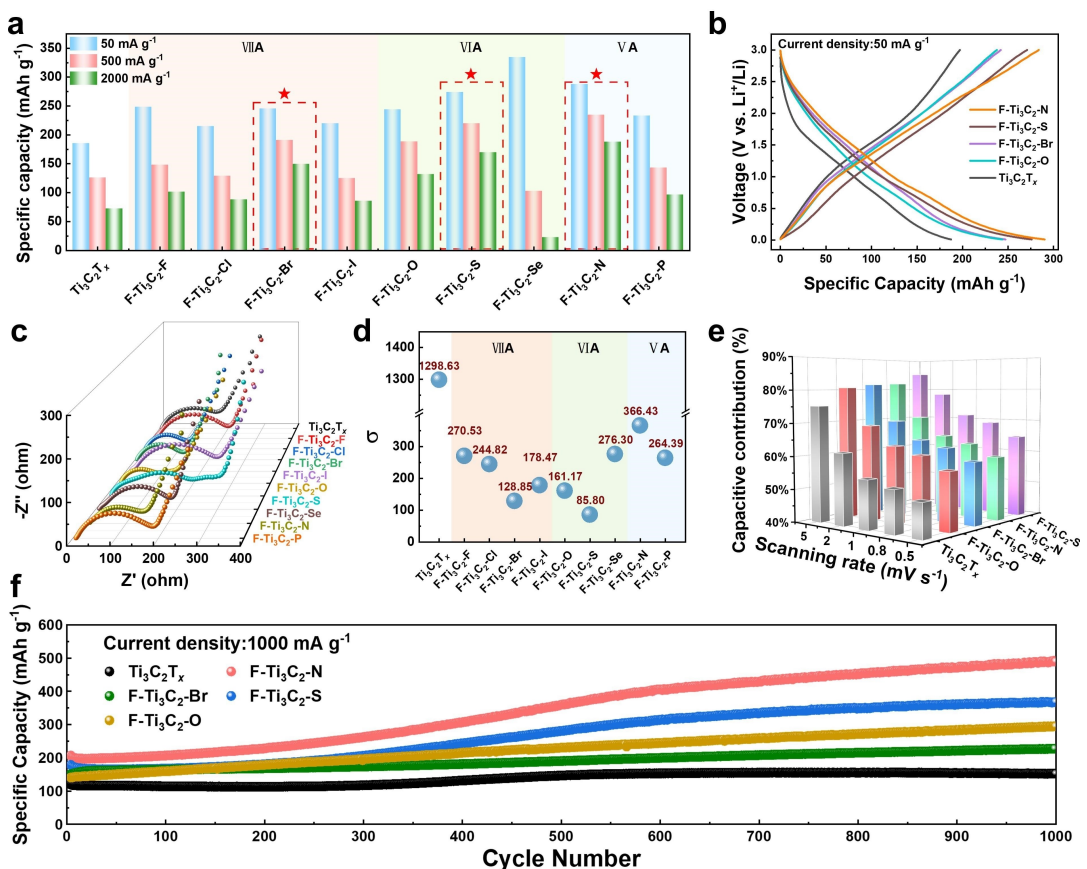


Figure 4. Comparison of electrochemical performance of 9 kinds of $\text{F-Ti}_3\text{C}_2\text{-X}$. (a) Average discharge specific capacities at 50, 500, and 2000 mA g^{-1} ; (b) Charge-discharge curves at 50 mA g^{-1} ; (c) EIS tests under the initial state of batteries; (d) Warburg coefficient (σ) calculation; (e) Capacitive contribution analysis based on CV test; (f) Cycling performance at 1000 mA g^{-1} .

poor, which may be related to the stability of Se termination. The ratios of the pseudocapacitive capacity contribution can be calculated for those F–Ti₃C₂–X based on the CV curves at different scan rates using the following equation:^[43–45]

$$I(V) = k_1 v + k_2 v^{1/2} \quad (1)$$

in which, $I(V)$ is current at a certain voltage; v is scan rate; k_1 and $k_2 v^{1/2}$ represent capacitance contribution and diffusion control processes, respectively. As shown in Figure 4e, F–Ti₃C₂–Br, F–Ti₃C₂–O, F–Ti₃C₂–S, and F–Ti₃C₂–N exhibit larger capacitance capacity contribution than the original Ti₃C₂T_x, with F–Ti₃C₂–S showing the highest capacitive ratios of 85% at 5 mVs⁻¹. This result indicates that the introduced redox reaction by the target terminations is a surface pseudocapacitance process. Figure 4f and Figure S12 display the cycling performance of the F–Ti₃C₂–X at 1000 mA g⁻¹ and 500 mA g⁻¹, respectively. Notably, F–Ti₃C₂–O, F–Ti₃C₂–S, and F–Ti₃C₂–N demonstrate excellent cycling performance without any decay. Among them, F–Ti₃C₂–N exhibits an impressive capacity retention of 238% after 1000 cycles along with a discharge capacity as high as 491.86 mAh g⁻¹, which significantly outperforms VII A terminations. The gradual increase in capacity can be attributed to the expansion in layer spacing (from 1.14 to 1.63 nm, Figure S13), which facilitates the accommodation of more Li ions between layers. This phenomenon is consistent with the findings reported in previous studies on layered electrode materials.^[46,47] In addition, the interlayer Van der Waals forces of F–Ti₃C₂–X with each functional group are different, thus the degrees of capacity increase vary. Significantly, the gradual increase in capacity is beneficial for enhancing the working life of energy storage devices when the F–Ti₃C₂–O, F–Ti₃C₂–S, and F–Ti₃C₂–N work as anodes.

Conclusions

In summary, we proposed a facile method for rapidly regulating surface function groups of Ti₃C₂T_x–MXenes via FJH reaction within 1 s. By changing modifying agents, 9 terminations, including VII A (F, Cl, Br, or I), VI A (O, S, or Se), and VA (N or P), either single or multiple, are effectively connected to MXenes, with a surface content up to 76%. The significant role of surface groups is confirmed in electrochemical Li-ion storage performance, demonstrating that VI A and V A terminations are superior to VII A. Particularly, F–Ti₃C₂–N, –S, and –O exhibit higher specific capacity and undecayed cycling performance. We posit that the efficient tuning approach for surface groups and the research findings lay the groundwork for designing physicochemical properties and optimizing the electrochemical performance of materials.

Experimental Section

Preparation of Original Ti₃C₂T_x

The Ti₃C₂T_x–MXene was prepared using the typical LiF/HCl etching method. 1 g LiF powder was dissolved in 40 ml of 9 M HCl in a PTFE bottle, and then 1 g Ti₃AlC₂ powder was added to the solution. The container was sealed and placed in a water bath at 45 °C for 40 h with magnetic stirring. After that, the resulting mixture was washed to neutrality with DI water through centrifugation to collect the multilayer Ti₃C₂T_x. Finally, few-layer Ti₃C₂T_x powder was obtained by sonication dispersion of the multilayer Ti₃C₂T_x and freeze-drying process. The Ti₃C₂T_x MXene powder obtained by this method usually shows a few-layer characteristic and the surface functional groups are generally –OH, –F, –Cl, and –O.

Preparation of Flash Ti₃C₂T_x (F–Ti₃C₂T_x) and Flash Ti₃C₂–X (F–Ti₃C₂–X)

The F–Ti₃C₂–X was prepared using the FJH technique. Firstly, Ti₃C₂T_x powder and compounds containing the surface target modifying elements were milled together, and then loaded into the quartz tubes used for the FJH reaction system. A low vacuum environment (-0.1 MPa) is provided for the reaction to prevent MXene oxidation and facilitate outgassing. The designed circuit can regulate the electric shock voltage and electrical energy, therefore controlling the reaction temperature. After the FJH reaction, the resulting samples were washed with different solvents that could dissolve the modifying agents. For example, selenium powder was washed with nitric acid, and red phosphorus was washed with NaOH. Subsequently, they were washed with DI water to obtain pure F–Ti₃C₂–X. The preparation of F–Ti₃C₂T_x follows the same procedure as that of F–Ti₃C₂–X without any modifying agents. The modifying agents used in this experiment and the FJH reaction conditions are listed in Table S3.

Materials Characterization

Surface chemical composition of MXene was analyzed by Fourier transform infrared spectrometer (FTIR, Bruker, ALPHA II) and X-ray photoelectron spectroscopy (XPS, Thermo Fisher Scientific, Escalab Xi+, using Al Ka radiation ($h\nu = 1486.6$ eV) and a monochromatic X-ray source with a 500-μm light spot size). X-ray diffraction (XRD) of MXene was investigated using a D/max-TTR III diffractometer with monochromatic Cu Kα radiation ($\lambda = 1.5418$ Å) at 40 KV and 150 mA. The morphology and elemental distribution of MXene before and after FJH treatment were observed using scanning electron microscopy (SEM, ZEISS, Gemini 300) and transmission electron microscopy (TEM, JEOL, JEM-2100), with energy dispersive spectroscopy (EDS, ZEISS, Smartedx). Lattice spacings and the crystal diffraction rings were measured and analyzed using Digital Micrograph software. The Thermogravimetry analysis (TG, NETZSCH, STA 449 F3) was used to analyze the antioxidant capacity of the samples.

Electrochemical Measurements

The anodes were prepared by uniformly dispersing MXene active materials, Super P as a conductive agent, and PVDF as a binder in NMP at a mass ratio of 8:1:1. Cu foil was used as the current collector, and the mass loading of MXene was 0.5–0.8 mg cm⁻². The electrolyte consisted of 1.0 M LiPF₆ in EC: DMC: EMC (1:1:1 vol %). The CR2032 coin-type half cells were assembled in an Ar-filled glove box following this order: anode (12 mm Φ), separator (16 mm Φ), lithium foil (15 mm Φ), spacer, spring tabs, and negative case.

The rate and cycling performance were tested between 0.01–3 V using the battery test system (NEWARE, CT-4008T). Electrochemical impedance spectroscopy (EIS) of the initial cells was tested at open circuit voltage using an electrochemical workstation (Ivium Technologies BV, Ivium-N-stat) with an amplitude of 5 mV over a frequency range from 100 kHz to 10 mHz. Cyclic voltammetry (CV) tests were performed at scan rates ranging from 0.5 to 5 mVs⁻¹ using the electrochemical workstation.

Acknowledgements

This work was supported by China Postdoctoral Science Foundation (2022TQ0291, 2022M712869), Frontier Exploration Projects of Longmen Laboratory of Henan (LMQYTSKT021), National Natural Science Foundation of China (52201283), and Key Research Projects of Henan Provincial Department of Education (23A530002).

Conflict of Interests

There are no conflicts to declare.

Data Availability Statement

Research data are not shared.

Keywords: surface functional groups • Ti₃C₂T_x MXene • flash Joule heating • anodes

- [1] V. Kamysbayev, A. S. Filatov, H. Hu, X. Rui, F. Lagunas, D. Wang, R. F. Klie, D. V. Talapin, *Science* **2020**, *369*, 979–983.
- [2] J. Zhou, P. Yang, P. A. Kots, M. Cohen, Y. Chen, C. M. Quinn, M. D. de Mello, J. Anibal Boscoboinik, W. J. Shaw, S. Caratzoulas, W. Zheng, D. G. Vlachos, *Nat. Commun.* **2023**, *14*, 2293.
- [3] M. Gyu Jung, G. Sambhaji Gund, Y. Gogotsi, H. Seok Park, *Batteries & Supercaps* **2020**, *3*, 354–360.
- [4] Y. Wang, T. Wang, Y. Mao, Z. Li, H. Yu, M. Su, K. Ye, D. Cao, K. Zhu, *Adv. Energy Mater.* **2024**, *n/a*, 2400353.
- [5] H. Ding, Y. Li, M. Li, K. Chen, K. Liang, G. Chen, J. Lu, J. Palisaitis, P. O. Å. Persson, P. Eklund, L. Hultman, S. Du, Z. Chai, Y. Gogotsi, Q. Huang, *Science* **2023**, *379*, 1130–1135.
- [6] Y. Wang, T. Guo, Z. Tian, K. Bibi, Y.-Z. Zhang, H. N. Alshareef, *Adv. Mater.* **2022**, *34*, 2108560.
- [7] J. Luo, X. Lu, E. Matios, C. Wang, H. Wang, Y. Zhang, X. Hu, W. Li, *Nano Lett.* **2020**, *20*, 7700–7708.
- [8] D. Yuan, Y. Dou, Z. Wu, Y. Tian, K.-H. Ye, Z. Lin, S. X. Dou, S. Zhang, *Chem. Rev.* **2022**, *122*, 957–999.
- [9] P. Liu, P. Xiao, M. Lu, H. Wang, N. Jin, Z. Lin, *Chin. Chem. Lett.* **2023**, *34*, 107426.
- [10] G. Dong, L. Li, P. Cui, A. M. A. Mohamed, K. Zhu, D. Cao, *Batteries & Supercaps* **2024**, *7*, e202300391.
- [11] M. Li, X. Li, G. Qin, K. Luo, J. Lu, Y. Li, G. Liang, Z. Huang, J. Zhou, L. Hultman, P. Eklund, P. O. Å. Persson, S. Du, Z. Chai, C. Zhi, Q. Huang, *ACS Nano* **2021**, *15*, 1077–1085.
- [12] J. Luo, E. Matios, H. Wang, X. Tao, W. Li, *InfoMat* **2020**, *2*, 1057–1076.
- [13] F. Ming, H. Liang, G. Huang, Z. Bayhan, H. N. Alshareef, *Adv. Mater.* **2021**, *33*, 2004039.
- [14] Y. Guo, Y. Gao, H. Chen, Q. Zhao, Q. Zhu, Z. Cao, B. Li, J. Shang, Z. Du, S. Yang, *Adv. Energy Mater.* **2023**, *13*, 2300890.
- [15] Z. Wang, Z. Xu, H. Huang, X. Chu, Y. Xie, D. Xiong, C. Yan, H. Zhao, H. Zhang, W. Yang, *ACS Nano* **2020**, *14*, 4916–4924.
- [16] Y. Xie, M. Naguib, V. N. Mochalin, M. W. Barsoum, Y. Gogotsi, X. Yu, K.-W. Nam, X.-Q. Yang, A. I. Kolesnikov, P. R. C. Kent, *J. Am. Chem. Soc.* **2014**, *136*, 6385–6394.
- [17] J. Zhao, N. Ma, T. Wang, N. Li, Y. Wang, J. Fan, *J. Mater. Chem. A* **2022**, *10*, 21611–21621.
- [18] H. Jing, H. Yeo, B. Lyu, J. Ryou, S. Choi, J.-H. Park, B. H. Lee, Y.-H. Kim, S. Lee, *ACS Nano* **2021**, *15*, 1388–1396.
- [19] N. Gupta, R. K. Sahu, T. Mishra, P. Bhattacharya, *J. Mater. Chem. A* **2022**, *10*, 15794–15810.
- [20] L. Liu, H. Zschiesche, M. Antonietti, B. Daffos, N. V. Tarakina, M. Gibilaro, P. Chamelot, L. Massot, B. Dupoyer, P.-L. Taberna, P. Simon, *Adv. Energy Mater.* **2023**, *13*, 2202709.
- [21] Y. Zheng, Y. Wang, J. Zhao, Y. Li, *ACS Nano* **2023**, *17*, 2487–2496.
- [22] J. Luo, J. Zheng, J. Nai, C. Jin, H. Yuan, O. Sheng, Y. Liu, R. Fang, W. Zhang, H. Huang, Y. Gan, Y. Xia, C. Liang, J. Zhang, W. Li, X. Tao, *Adv. Funct. Mater.* **2019**, *29*, 1808107.
- [23] N. Liu, Q. Li, H. Wan, L. Chang, H. Wang, J. Fang, T. Ding, Q. Wen, L. Zhou, X. Xiao, *Nat. Commun.* **2022**, *13*, 5551.
- [24] W. Chen, C. Ge, J. T. Li, J. L. Beckham, Z. Yuan, K. M. Wyss, P. A. Advincula, L. Eddy, C. Kittrell, J. Chen, D. X. Luong, R. A. Carter, J. M. Tour, *ACS Nano* **2022**, *16*, 6646–6656.
- [25] O. Vieira, R. S. Ribeiro, J. L. Diaz de Tuesta, H. T. Gomes, A. M. T. Silva, *Chem. Eng. J.* **2022**, *428*, 131399.
- [26] S. Dong, Y. Song, M. Su, G. Wang, Y. Gao, K. Zhu, D. Cao, *Chem. Eng. J.* **2024**, *481*, 147988.
- [27] W. Chen, Z. Wang, K. V. Bets, D. X. Luong, M. Ren, M. G. Stanford, E. A. McHugh, W. A. Algozeeb, H. Guo, G. Gao, B. Deng, J. Chen, J. T. Li, W. T. Carsten, B. I. Yakobson, J. M. Tour, *ACS Nano* **2021**, *15*, 1282–1290.
- [28] C. Wu, X. Luo, X. Yu, X. Yu, K. Lin, M. Li, Z. Li, Y. Cao, Y. Zhou, *Chin. Chem. Lett.* **2023**, *34*, 107881.
- [29] Y.-Z. Fang, S. Liang, X. Zhang, J. Sang, S. Gao, Z. Zhang, K. Zhu, D. Cao, Z. Zhou, *Chem. Commun.* **2022**, *58*, 9373–9376.
- [30] P. A. Advincula, W. Meng, L. J. Eddy, P. Z. Scotland, J. L. Beckham, S. Nagarajaiah, J. M. Tour, *ACS Appl. Mater. Interfaces* **2024**, *16*, 1474–1481.
- [31] S. Xu, C. Liu, X. Jiang, X. Wang, S. Zhang, Y. Zhang, Q. Wang, W. Xiong, J. Zhang, *J. Hazard. Mater.* **2023**, *444*, 130450.
- [32] M. Shi, R. Wang, L. Li, N. Chen, P. Xiao, C. Yan, X. Yan, *Adv. Funct. Mater.* **2023**, *33*, 2209777.
- [33] L.-Å. Näslund, P. O. Å. Persson, J. Rosen, *J. Phys. Chem. C* **2020**, *124*, 27732–27742.
- [34] C. Wang, S. Wei, P. Zhang, K. Zhu, P. Song, S. Chen, L. Song, *Chin. Chem. Lett.* **2020**, *31*, 969–979.
- [35] S. Doo, A. Chae, D. Kim, T. Oh, T. Y. Ko, S. J. Kim, D.-Y. Koh, C. M. Koo, *ACS Appl. Mater. Interfaces* **2021**, *13*, 22855–22865.
- [36] C. E. Park, G. H. Jeong, J. Theerthagiri, H. Lee, M. Y. Choi, *ACS Nano* **2023**, *17*, 7539–7549.
- [37] P. Zhang, Y. Li, Y. Zhang, R. Hou, X. Zhang, C. Xue, S. Wang, B. Zhu, N. Li, G. Shao, *Small Methods* **2020**, *4*, 2000214.
- [38] Y.-Z. Fang, S. Liang, X. Zhang, J. Sang, S. Gao, Z. Zhang, K. Zhu, D. Cao, Z. Zhou, *Chem. Commun.* **2022**, *58*, 9373.
- [39] G. Valuoruthu, R. Panigrahi, M. Saraf, C. E. Shuck, B. S. Mallik, N. Kurra, Y. Gogotsi, *Batteries & Supercaps* **2023**, *6*, e20230009.
- [40] S. Kumar, A. Mondal, V. Panwar, R. Shekhawat, A. Misra, *Batteries & Supercaps* **2024**, *7*, e202300393.
- [41] S. Alancherry, K. Bazaka, I. Levcchenko, A. Al-jumaili, B. Kandel, A. Alex, F. C. Robles Hernandez, O. K. Varghese, M. V. Jacob, *ACS Appl. Mater. Interfaces* **2020**, *12*, 29594–29604.
- [42] P. Pandey, S. Bhowmick, M. Qureshi, *ACS Appl. Mater. Interfaces* **2023**, *15*, 39435–39447.
- [43] C. Han, J. Zhu, K. Fu, D. Deng, W. Luo, L. Mai, *Chem. Commun.* **2022**, *58*, 791–794.
- [44] Q. Wei, Q. Li, Y. Jiang, Y. Zhao, S. Tan, J. Dong, L. Mai, D.-L. Peng, *Nano-Micro Lett.* **2021**, *13*, 55.
- [45] B. Zhang, A. Boretti, S. Castelletto, *Chem. Eng. J.* **2022**, *435*, 134959.
- [46] Y.-Z. Fang, R. Hu, K. Zhu, K. Ye, J. Yan, G. Wang, D. Cao, *Adv. Funct. Mater.* **2020**, *30*, 2005663.
- [47] J. Guo, Y. Li, J. Meng, K. Pedersen, L. Gurevich, D.-I. Stroe, *J. Energy Chem.* **2022**, *74*, 34–44.

Manuscript received: April 23, 2024

Revised manuscript received: May 12, 2024

Accepted manuscript online: May 14, 2024

Version of record online: June 20, 2024